Flight Path Angle Controller Design Based on Adaptive Backstepping Terminal Sliding Mode Control Method

Yang Wei(✉), Haojun Xu, Yuan Xue, Zhe Li, and Hongfeng Tian

Aeronautics Engineering College,
Air Force Engineering University, Xi'an, China
15339171636@163.com

Abstract. A method of controlling flight-path angle via adaptive backstepping terminal sliding mode is presented. At the first two steps of the design process of controller, Radial Basis Function (RBF) neural networks are employed to approximate the unknown parameters uncertainty online and the dynamic surface control is combined with backstepping design technique to design the virtual controller, so that the explosion of complexity in traditional backstepping design is avoided perfectly. In the last step, the high-order sliding mode control law is designed by the non-singular terminal sliding mode to eliminate the chattering and make the system robust to uncertainties. It is proved by Lyapunov method that all signals in the closed-loop system are semi-global uniform ultimately bounded, and the tracking error can be adjusted by adjusting the controller parameters to converge into a small neighborhood of zero. Finally, the simulation results demonstrate the validity of the proposed method.

Keywords: Flight-path angle · Adaptive backstepping terminal sliding mode · RBF neural networks · Dynamic surface control

1 Introduction

The control problem of uncertain systems has always been one of the research hotspots in the control field. As described in Ref. [1], the flight path tracking control for aircraft poses several difficulties such as the highly coupled nonlinearity of the six-degree-of-freedom (6DOF) flight dynamic system and the model errors of system parameters related to many aerodynamic coefficients. The traditional linear control techniques (PID, LQR, etc.) may not work very well.

Various control techniques and approaches have been proposed for flight path angle tracking problem. In Ref. [2], the author adopted a barrier Lyapunov function (BLF) backstepping method to design the flight path angle tracking controller with attack angle constraints. In Ref. [3], the virtual control is designed with nominal feedback and neural network (NN) approximation via backstepping for hypersonic vehicle. In Ref. [4], a neural network based adaptive dynamic surface control is proposed for the aircraft longitudinal flight path angle. In Ref. [5], the nonlinear backstepping technique applied to the flight-path angle tracking control problem. All of the

X. Zhang (Ed.): APISAT 2018, LNEE 459, pp. 2466–2479, 2019.
https://doi.org/10.1007/978-981-13-3305-7_197

above literatures had used backstepping method. Also, the variable structure control methods had been used in flight-path angle tracking. In Ref. [6], a recursive sliding mode control method with nonlinear gains is proposed for the flight-path angle tracking during the landing phase.

Although variable structure controllers are simple in design and have been widely used for matched uncertain systems, the robustness of variable structure control is difficult to be guaranteed for the non-matching uncertain systems. A more successful control strategy is the adaptive backstepping method [7–9]. It can realize the global adjustment by designing the controller through the stepwise correction algorithm. However, the adaptive backstepping method require that the system uncertainty can be parameterized, and there is a problem of "computation expansion". As the relative order of the controlled object increases, the control law is highly nonlinear and highly complex [10, 11], which makes the controller difficult to implement.

In recent years, some scholars have combined variable structure control with adaptive backstepping, which makes the system robust to matching uncertainty and non-matching uncertainty, and has achieved many results. Ref. [12] presents a multiple sliding mode robust adaptive control method similar to the backstepping algorithm for a class of non-regular high-order nonlinear system with matching uncertainties, but the uncertainty still needs to be parameterizable. Ref. [13] improved the final step of the standard inversion algorithm using the sliding mode control method and applied it to the missile control system. Ref. [14] designed an adaptive backstepping variable structure controller for a class of minimum phase affine nonlinear systems. The controller studies the adjustment problem of the system under the unknown disturbance action and allows the nonparametric matching uncertainty in the last equation of the system. Ref. [15] presents a state reference adaptive control algorithm combined with linear sliding mode for a class of triangular structure non-matching uncertain systems. In Ref. [16], the second-order sliding mode control method is applied to the auxiliary system of the last two steps of the adaptive backstepping method, which reduces the calculation amount of the algorithm and allows the non-parametric uncertainty of the last two equations of the system, but since the relative order of the system is two, this method does not eliminate the chattering phenomenon.

In this paper, an adaptive backstepping terminal sliding mode control method is proposed for a flight path angle control system. The first two step of the backstepping control combines the adaptive law to estimate the unknown parameters of the system to suppress the non-matching disturbance. The last step adopts a special non-singular terminal sliding mode to replace the traditional linear sliding mode. The control strategy based on high-order sliding mode is designed to remove the control chattering, and make the last state of the system converge in a finite time, and the remaining states and parameter estimates asymptotically converge. The control method proposed in this paper can improve the convergence speed and steady-state tracking accuracy of the system, and make the system match the uncertainty.

2 System Definition

Since only the longitudinal movements of the aircraft is considered here, we can assume that $\phi = \psi = \beta = p = r = 0$. That is, there is no rolling, yawing and side slipping motion. Furthermore, when $\beta = \phi = 0$, the flight path angle γ can be defined as

$$\gamma = \theta - \alpha \tag{1}$$

So the longitudinal aircraft dynamic equations related to flight path angle can be derived from the full, 6DOF, nonlinear, rigid-body equations. The equations used in this paper are as follow [8]

$$\begin{cases} \dot{\gamma} = \frac{1}{mV_t}(L + F_T \sin\alpha - mg\cos\gamma) \\ \dot{\alpha} = \frac{1}{mV_t}(-L - F_T \sin\alpha + mg\cos\gamma) + q \\ \dot{\theta} = q \\ \dot{q} = \frac{M}{I_y} \end{cases} \tag{2}$$

where V_t is the flight velocity, γ is the flight path angle, α is the angle of attack, θ is the pitch angle, q is the pitch rate, F_T is the thrust force, δ_e is the elevator deflection, g is the gravitational constant, m and I_y are the mass and the pitch moment of inertia, L and M represent aerodynamic lift and pitch moment, and can be modeled as:

$$L = \bar{q}SC_L = \frac{1}{2}\rho V_t^2 S(C_{L0} + C_{L\alpha}\alpha) \tag{3}$$

$$M = \bar{q}S\bar{c}C_m = \frac{1}{2}\rho V_t^2 S\bar{c}(C_{m0} + C_{m\alpha}\alpha + \frac{\bar{c}}{2V_t}(C_{mq}q + C_{m\dot{\alpha}}\dot{\alpha}) + C_{m\delta_e}\delta_e) \tag{4}$$

where $\bar{q} = 0.5\rho V_t^2$ is the dynamical pressure, ρ is the density of air; S is the wing area; C_L is lift coefficient; M is the aerodynamic contributions to pitching moment; I_y is the pitch moment of inertia; $\bar{c}$ is the mean aerodynamic chord; C_{m0}, $C_{m\alpha}$, C_{mq}, $C_{m\dot{\alpha}}$, $C_{m\delta_e}$ are the components of the pitch moment coefficient. Also, for small α, the approximation $\sin\alpha = \alpha$ is used to simplify the Eq. (2).

Choosing α as an intermediate control variable, the dynamics of the triple (γ, α, q) can be expressed in strict-feedback form as follows:

$$\begin{cases} \dot{x}_1 = g_5 x_2 + f_1(x_1) \\ \dot{x}_2 = x_3 + f_2(x_1, x_2) \\ \dot{x}_3 = g_3 u + f_3(x_2, x_3) \end{cases} \tag{5}$$

where $f_1(x_1) = -g_6 - g_4 \cos x_1,\ f_2(x_1, x_2) = g_6 + g_4 \cos x_1 - g_5 x_2,\ f_3(x_2, x_3) = g_0 + g_1 x_3 + g_2 x_2 + g_7 \dot{x}_2$. The expressions of $g_i (i = 0, \cdots 7)$ are as follows:

$$
\begin{aligned}
&g_0 = \frac{1}{I_y} \bar{q} S \bar{c} C_{m0}, g_1 = \frac{1}{2 V_t I_y} \bar{q} S \bar{c}^2 C_{mq}, g_2 = \frac{1}{I_y} \bar{q} S \bar{c} C_{m\alpha}, \\
&g_3 = \frac{1}{I_y} \bar{q} S \bar{c} C_{m\delta_e}, g_4 = \frac{g}{V_t}, g_5 = \frac{\bar{q} S}{m V_t} C_{L_\alpha} + \frac{F_T}{m V_t}, g_6 = -\frac{\bar{q} S}{m V_t} C_{L_0}, \\
&g_7 = \frac{1}{2 V_t I_y} \bar{q} S \bar{c}^2 C_{m\dot{\alpha}}
\end{aligned}
$$

The aerodynamic parameters of an aircraft are rarely, if ever, known exactly but approximations to them are certainly available. In order to model parameter uncertainty and time-varying external disturbances, $\psi_i(\bar{x}_i, t)(i = 1, 2, 3)$ are added to the Eq. (5), $\bar{x}_i = [x_1, x_2, \cdots, x_i]^T$. The final version of the system can be modeled as:

$$
\begin{cases}
\dot{x}_1 = g_5 x_2 + f_1(x_1) + \psi_1(\bar{x}_1) \\
\dot{x}_2 = x_3 + f_2(x_1, x_2) + \psi_2(\bar{x}_2) \\
\dot{x}_3 = g_3 u + f_3(x_2, x_3) + \Delta f(\bar{x}_3, t) \\
y = x_1
\end{cases}
\tag{6}
$$

where $\Delta f(\bar{x}_3, t)$ represents unknown parameter uncertainty and time-varying external disturbances for the system, $\psi_i(\bar{x}_i)(i = 1, 2)$ represents the unknown nonlinear function. And the expressions of $\psi_i(\bar{x}_i, t)(i = 1, 2)$ are as follows:

$$
\begin{cases}
\psi_1(\bar{x}_1) = -\Delta g_6 - \Delta g_4 \cos x_1 + \Delta g_5 x_2 \\
\psi_2(\bar{x}_2) = \Delta g_6 + \Delta g_4 \cos x_1 - \Delta g_5 x_2 \\
\Delta f(\bar{x}_3, t) = \Delta g_3 u + \Delta g_0 + \Delta g_1 x_3 + \Delta g_2 x_2 + \Delta g_7 \dot{x}_2 + d(t)
\end{cases}
\tag{7}
$$

where Δg_i represent aerodynamic parameter uncertainty.

The actuator model used in this paper can be simplified to three parts: first-order inertia link, rate limiter and position limiter. As shown in Fig. 1, T is time constant of the first-order inertia link, and $1/(Ts + 1)$ is the transfer function of actuator.

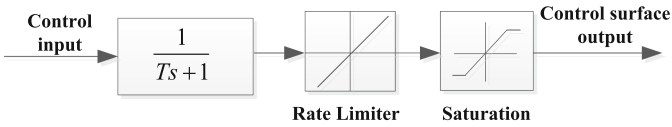

Fig. 1. The schematic diagram of dynamics model for actuator

The detailed parameters of rate limiter and position limiter can be set referring to Ref. [17]. In this paper, these parameters are set as follows. T = 0.05 s. The maximum value of control input is 25°, the minimum value of control input is −10°. The maximum rate limit is 20 deg/s, and the minimum rate limit is −20 deg/s.

Assumption 1. $\psi_i(\bar{x}_i)(i = 1, 2)$, $\Delta f(\bar{x}_3, t)$ and their derivatives are bounded.

Assumption 2. The reference signal x_{1d} belongs to a compact set

$$x_{1d} \in \Omega_d = \{[x_{1d}, \dot{x}_{1d}, \ddot{x}_{1d}]^T : x_{1d}^2 + \dot{x}_{1d}^2 + \ddot{x}_{1d}^2 \leq \xi\} \tag{8}$$

where $\xi > 0$ is a known constant.

The goal of control is that designing the control surface input u enables the flight path angle x_1 to accurately track the desired flight path angle command x_{1d} (γ_d).

3 Control Law Design

In this paper, we use adaptive backstepping terminal sliding mode control method to design control law for flight path angle tracking. Next is the main design process of the adaptive backstepping terminal sliding mode control method.

Here introducing the controller parameters $k_i, \tau_j > 0(i = 1, 2; j = 1, 2)$, $\Delta > 0$, the specific design process of the control law is as follows.

First define the tracking error of the system as:

$$\begin{cases} e_1 = x_1 - x_{1d} \\ e_2 = x_2 - \alpha_1 \\ e_3 = x_3 - \alpha_2 \end{cases} \tag{9}$$

where α_i (i = 1, 2) is the filtered virtual control volume of the i-th order subsystem.

Step 1. According to the differential equations and tracking errors of the first-order subsystem defined before, we have:

$$\dot{e}_1 = \dot{x}_1 - \dot{x}_{1d} = g_5 x_2 + f_1(x_1) + \psi_1(\bar{x}_1) - \dot{x}_{1d} \tag{10}$$

Here the RBF neural network $h_1(x_1) = \theta_1^{*T}\xi_1(x_1) + \sigma_1$ is used to approximate the unknown function $\psi_1(\bar{x}_1)$. θ_1^* is the ideal weight, $\left\|\theta_1^*\right\| \leq \theta_M$. σ_1 is the approximation error, $|\sigma_1| \leq \sigma_M$. We can get:

$$\dot{e}_1 = g_5 x_2 + f_1(x_1) + \theta_1^{*T}\xi_1(x_1) + \sigma_1 - \dot{x}_{1d} \tag{11}$$

Define the Lyapunov function $V_1 = \frac{1}{2}e_1^2$. In order to make sure $\dot{V}_1 = e_1\dot{e}_1 = e_1 \left[g_5 x_2 + f_1(x_1) + \theta_1^{*T}\xi_1(x_1) + \sigma_1 - \dot{x}_{1d}\right] \leq 0$, the virtual control volume is designed as follows

$$\beta_1 = \frac{1}{g_5}\left[-k_1 e_1 - f_1(x_1) - \hat{\theta}_1^T\xi_1(x_1) + \dot{x}_{1d}\right] \tag{12}$$

In the Eq. (14), k_1 is a positive design parameter. $\hat{\theta}$ is the estimate of the weight θ_1^*. The adaptive law for the weight of the first RBF network is as follows

$$\dot{\hat{\theta}}_1 = \boldsymbol{\Gamma}_1(\xi_1 e_1 - \eta_1 \hat{\theta}_1) \tag{13}$$

where η_1 is a positive real number, and $\boldsymbol{\Gamma}_1 = \boldsymbol{\Gamma}_1^T > 0$ is an adaptive gain matrix.

The traditional backstepping design method will make the number of items expanding in the process of differential differentiation of virtual control, which will result in a complicated design process of the control law. In order to avoid deriving the desired virtual control in the next step, a dynamic surface control technique is introduced to reduce the design complexity of the control law and the virtual control law is filtered by a first-order low-pass filter. The dynamic equation of the filter is:

$$\tau_1 \dot{\alpha}_1 + \alpha_1 = \beta_1, \alpha_1(0) = \beta_1(0) \tag{14}$$

where τ_1 is the time constant of the filter.

Step 2. According to the tracking error of the second-order subsystem, we have:

$$\dot{e}_2 = \dot{x}_2 - \dot{\alpha}_1 = x_3 + f_2(x_1, x_2) + \psi_2(\bar{x}_2) - \dot{\alpha}_1 \tag{15}$$

The RBF neural network $h_2(\bar{x}_2) = \theta_2^{*T}\xi_2(\bar{x}_2) + \sigma_2$ is used to approximate the unknown function $\psi_2(\bar{x}_2)$. Then we can get:

$$\dot{e}_2 = \dot{x}_2 - \dot{\alpha}_1 = x_3 + f_2(x_1, x_2) + \theta_2^{*T}\xi_2(\bar{x}_2) + \sigma_2 - \dot{\alpha}_1 \tag{16}$$

The virtual control volume and the adaptive law for the weight of the second RBF network are designed as follows

$$\beta_2 = -k_2 e_2 - f_2(x_1, x_2) - \hat{\theta}_2^T \xi_2(\bar{x}_2) + \dot{\alpha}_1 \tag{17}$$

$$\dot{\hat{\theta}}_2 = \boldsymbol{\Gamma}_2(\xi_2 e_2 - \eta_2 \hat{\theta}_2) \tag{18}$$

where $k_2, \eta_2 > 0$, $\boldsymbol{\Gamma}_2 = \boldsymbol{\Gamma}_2^T > 0$.

Also, the virtual control volume β_2 is filtered by a first-order low-pass filter. The dynamic equation of the filter is:

$$\tau_2 \dot{\alpha}_2 + \alpha_2 = \beta_2, \quad \alpha_2(0) = \beta_2(0) \tag{19}$$

where τ_2 is the time constant of the filter.

Step 3. In order to make the state tracking error e_3 converge to zero in a finite time, and improve the convergence speed and steady-state tracking accuracy of the error system, the non-singular terminal sliding surface is designed in the following

$$s = e_3 + \lambda \dot{e}_3^{p/q} \tag{20}$$

where $\lambda > 0$, p and q are positive odd numbers, and $1 < p/q < 2$.

Suppose that at t_n time, s converges to zero, that is, $s(t) = 0, t \geq t_n$. Then e_3 and $\dot{e}_3$ will converge to zero in a finite time, and the convergence time is

$$t_s = t_n + \lambda^{\frac{q}{p}} \frac{p}{p-q} |e_3(t_n)|^{\frac{p-q}{p}} \tag{21}$$

At this time, the system will remain in the second-order sliding mode. According to the Eq. (21), the convergence speed of e_3 can be effectively adjusted by selecting parameters p and q. On this basis, the paper uses the terminal sliding mode combined with the high-order sliding mode control method to design the final control law, which is shown as below

$$u = u_1 + u_2 \tag{22}$$

$$u_1 = -\frac{1}{g_3}[f_3(x_2, x_3) - \dot{\alpha}_2] \tag{23}$$

$$u_2 = -\frac{1}{g_3}\{\int_0^t [\frac{q}{\lambda p} \dot{e}_3^{2-p/q} + \rho_1 \text{sgn } s + \rho_2 s] d\tau\} \tag{24}$$

where $\rho_1 > \left|\Delta \dot{f}(\bar{x}_3, t)\right|$, $\rho_2 > 0$ are the parameters to be designed.

4 Stability Analysis

First define the filter error as:

$$y_i = \alpha_i - \beta_i \, (i = 1, 2) \tag{25}$$

From the Eqs. (14) and (19), we have

$$\dot{\alpha}_i = -\frac{y_i}{\tau_i} \tag{26}$$

The weight estimation error is defined as

$$\tilde{\theta}_i = \hat{\theta}_i - \theta_i^* (i = 1, 2) \tag{27}$$

The derivative of each order subsystem errors are

$$\begin{aligned} \dot{e}_1 &= g_5 x_2 + f_1(x_1) + \theta_1^{*T} \xi_1 + \sigma_1 - \dot{x}_{1d} = g_5(e_2 + y_1 + \beta_1) + f_1(x_1) + \theta_1^{*T} \xi_1 + \sigma_1 - \dot{x}_{1d} \\ &= g_5(e_2 + y_1 + \tfrac{1}{g_5}\left[-k_1 e_1 - f_1(x_1) - \hat{\theta}_1^T \xi_1 + \dot{x}_{1d}\right]) + f_1(x_1) + \theta_1^{*T} \xi_1 + \sigma_1 - \dot{x}_{1d} \\ &= -k_1 e_1 + g_5(e_2 + y_1) - \tilde{\theta}_1^T \xi_1 + \sigma_1 \end{aligned} \tag{28}$$

$$\dot{e}_2 = -k_2 e_2 + e_3 + y_2 - \tilde{\theta}_2^T \xi_2 + \sigma_2 \tag{29}$$

$$\dot{e}_3 = g_3 u_2 + \Delta f \tag{30}$$

The derivative of filter errors are

$$\dot{y}_1 = -\frac{y_1}{\tau_1} - \dot{\beta}_1 = -\frac{y_1}{\tau_1} - \frac{1}{g_5}\left[-k_1\dot{e}_1 - \dot{f}_1(x_1) - \dot{\hat{\theta}}_1^T\xi_1(x_1) + \ddot{x}_{1d}\right] \tag{31}$$

$$\dot{y}_2 = -\frac{y_2}{\tau_2} - \dot{\beta}_2 = -\frac{y_2}{\tau_2} - \frac{1}{g_5}\left[-k_2e_2 - f_2(x_1, x_2) - \hat{\theta}_2^T\xi_2(\bar{x}_2) + \dot{\alpha}_1\right] \tag{32}$$

Based on Assumptions 1–2, clearly, there are continuous functions B_i satisfying the following in equation

$$\left|\dot{\beta}_i\right| \le B_i(e_1, e_2, y_1, y_2, \tilde{\theta}_1, \tilde{\theta}_2, x_{1d}, \dot{x}_{1d}, \ddot{x}_{1d}) \tag{33}$$

According to the Eqs. (31)–(33) we obtain that

$$y_i\dot{y}_i \le -\frac{y_i^2}{\tau_i} + |y_i|B_i \le -\frac{y_i^2}{\tau_i} + \frac{1}{2}y_i^2 + \frac{1}{2}B_i^2 \tag{34}$$

Define the Lyapunov function of the whole system as

$$V = V_2 + V_3 \tag{35}$$

where $V_1 = \frac{1}{2}e_1^2 + \frac{1}{2}y_1^2 + \frac{1}{2}\tilde{\theta}_1^T\boldsymbol{\Gamma}_1^{-1}\tilde{\theta}_1$, $V_2 = V_1 + \frac{1}{2}e_2^2 + \frac{1}{2}y_2^2 + \frac{1}{2}\tilde{\theta}_2^T\boldsymbol{\Gamma}_2^{-1}\tilde{\theta}_2$, $V_3 = \frac{1}{2}s^2$.

First, the derivative of V_1 is

$$\begin{aligned}
\dot{V}_1 &= e_1\dot{e}_1 + y_1\dot{y}_1 + \tilde{\theta}_1^T\boldsymbol{\Gamma}_1^{-1}\dot{\hat{\theta}}_1 \\
&= g_5e_1e_2 + g_5e_1y_1 - k_1e_1^2 - e_1\tilde{\theta}_1^T\xi_1 + e_1\sigma_1 + y_1\dot{y}_1 + \tilde{\theta}_1^T\boldsymbol{\Gamma}_1^{-1}\dot{\hat{\theta}}_1 \\
&\le -k_1e_1^2 + g_5e_1e_2 + e_1\sigma_1 + g_5|e_1||y_1| - \frac{y_1^2}{\tau_1} + \frac{1}{2}y_1^2 + \frac{1}{2}B_1^2 - \tilde{\theta}_1^T\boldsymbol{\Gamma}_1^{-1}[\boldsymbol{\Gamma}_1\xi_1e_1 - \dot{\hat{\theta}}_1]
\end{aligned} \tag{36}$$

Let $k_1 = k_{10} + k_{11}, k_{10} - g_5 > 0, k_{11} > 0$, and based on the Young's inequality, these inequalities can be derived as follows

$$\begin{aligned}
&|e_1||y_1| \le \frac{1}{2}e_1^2 + \frac{y_1^2}{2}, -\eta_1\tilde{\theta}_1^T\hat{\theta}_1 \le \frac{\eta_1}{2}\left\|\theta_1^*\right\|^2 - \frac{\eta_1}{2}\left\|\tilde{\theta}_1\right\|^2, -k_{11}e_1^2 + e_1\sigma_1 \le \\
&\quad -k_{11}e_1^2 + e_1|\sigma_1| \le \frac{\sigma_1^2}{4k_{11}} \le \frac{\sigma_1^{*2}}{4k_{11}}
\end{aligned}$$

So we can get

$$\dot{V}_1 \le -k_1^*e_1^2 + g_5e_1e_2 + \frac{1+g_5}{2}y_1^2 - \frac{y_1^2}{\tau_1} + \frac{1}{2}B_1^2 + \frac{\eta_1}{2}\left\|\theta_1^*\right\|^2 - \frac{\eta_1}{2}\left\|\tilde{\theta}_1\right\|^2 + \frac{\sigma_1^{*2}}{4k_{11}} \tag{37}$$

where $k_1^* = k_1 - \frac{g_5}{2}$. In the same way, the derivative of V_2 meet the following inequality

$$\begin{aligned}\dot{V}_2 &\le \dot{V}_1 - (k_{20}-1)e_2^2 + e_2e_3 + y_2^2 - \tfrac{y_2^2}{\tau_2} + \tfrac{1}{2}B_2^2 + \tfrac{\eta_2}{2}\left\|\theta_2^*\right\|^2 - \tfrac{\eta_2}{2}\left\|\tilde{\theta}_2\right\|^2 + \tfrac{\sigma_2^{*2}}{4k_{21}} \\ &\le -(k_1^* - \tfrac{g_5}{2})e_1^2 - (k_2^* - \tfrac{g_5}{2})e_2^2 + e_2e_3 + \tfrac{1+g_5}{2}y_1^2 + y_2^2 + \sum_{i=1}^{2}(-\tfrac{y_i^2}{\tau_i} + \tfrac{1}{2}B_i^2 + \tfrac{\eta_i}{2}\left\|\theta_i^*\right\|^2 - \tfrac{\eta_i}{2}\left\|\tilde{\theta}_i\right\|^2 + \tfrac{\sigma_i^{*2}}{4k_{i1}})\end{aligned} \tag{38}$$

where $k_2 = k_{20} + k_{21}, k_{20} > 1, k_{21} > 0, k_2^* = k_{20} - 1$.

Form the Eq. (38), we can know that if the designed control law makes e_3 converge to zero, then

$$\dot{V}_2 \le \mu V_2 + \varepsilon \tag{39}$$

where μ and ε are positive real number, and defined as

$$\begin{aligned}\mu &= \min_{1\le i\le 2}\left\{2k_i^* - g_5, \frac{\eta_i}{\lambda_{\max}(\boldsymbol{\Gamma}_i^{-1})}\right\}, \quad \varepsilon \\ &= \sum_{i=1}^{2}(\omega y_i^2 - \frac{y_i^2}{\tau_i} + \frac{1}{2}B_i^2 + \frac{\eta_i}{2}\left\|\theta_i^*\right\|^2 + \frac{\sigma_i^{*2}}{4k_{i1}}), \quad \omega = \max(\frac{1+g_5}{2}, 1)\end{aligned}$$

The above analysis shows that if the state tracking error e_3 converges to zero, then it can guarantee that the subsystems composed of e_1, e_2 are stable.

Next, the derivative of V_3 is

$$\dot{V}_3 = s\dot{s} = s(\dot{e}_3 + \lambda\frac{p}{q}\dot{e}_3^{p/q-1}\ddot{e}_3) \tag{40}$$

Substituting the Eqs. (24) and (30) into the above equation, we can get

$$\begin{aligned}&\dot{V}_s = s\dot{s} = s(\dot{e}_3 + \lambda\tfrac{p}{q}\dot{e}_3^{p/q-1}\ddot{e}_3) = s(\dot{e}_3 + \lambda\tfrac{p}{q}\dot{e}_3^{p/q-1}(\dot{\psi}_3 - \tfrac{q}{\lambda p}\dot{e}_3^{2-p/q} - \rho_1\mathrm{sgn}s - \rho_2 s) \\ &= s\lambda\tfrac{p}{q}\dot{e}_3^{p/q-1}(\dot{\psi}_3 - \rho_1\mathrm{sgn}s - \rho_2 s) \\ &\le -\lambda\tfrac{p}{q}\dot{e}_3^{p/q-1}\rho_2 s^2\end{aligned} \tag{41}$$

When $s \ne 0$, because $1 < p/q < 2$, $\dot{e}_3^{p/q-1} \ge 0$ satisfied, so $\dot{V}_s \le 0$. If and only when $\dot{e}_3 = 0$, $\dot{V}_s = 0$. It can be proved that it is not a stable state, and the system will not remain in this state all the time, that is, it cannot be maintained steadily. Therefore, the system will reach the non-singular terminal sliding surface in a limited time, and the state tracking error will also converge in a limited time.

When e_3 converges to zero, the Eq. (40) holds, and multiply $e^{\mu t}$ to both sides of the Eq. (39) and we can get

$$\frac{d}{dt}(V_2(t)e^{\mu t}) \le e^{\mu t}\varepsilon \tag{42}$$

Define $\phi = \varepsilon/\mu$, then

$$V_2(t) \leq \phi + [V_2(0) - \phi]e^{-\mu t} \leq \phi + V_2(0) \tag{43}$$

It can be seen from the Eq. (43) that the state e_i, $\tilde{\theta}_i$ of the first two order subsystem is semi-global uniform ultimately bounded, and thus $\hat{\theta}_i$ is bounded. By analogy, all states of the closed-loop system x_1, x_2, x_3 are bounded. So, the tracking error can be adjusted by adjusting the controller parameters to converge into a small neighborhood of zero.

5 Simulation Result

In this subsection, we simulate the adaptive backstepping terminal sliding mode controller for two cases: the nominal situation and the non-nominal situation.

5.1 Case1: The Nominal Situation

In this simulation case, the flight path angle command is set as: $\gamma_d = x_{1d} = 5\sin(\frac{\pi}{10}t)$. There are no parameters uncertainty and time-varying external disturbances in the nominal simulation case. The main parameters for aircraft and control parameters are showed in Table 1.

Table 1. The main parameters for aircraft and control parameters

Parameters	Value
m (kg)	43900
S (m^2)	121.86
I_y ($kg.m^2$)	2069903.25
$\bar{c}$ (m)	3.4426
V_t (m/s)	70
F_T (N)	61837
k_1	3.1
k_2	2
λ	0.01
p	5
q	3
ρ_1	0.05
ρ_2	25
τ_1 τ_2	0.01
$\boldsymbol{\Gamma}_1$ $\boldsymbol{\Gamma}_2$	0.5$\boldsymbol{I}$ ($\boldsymbol{I}$ is unit matrix)
η_1 η_2	0.04

Considering that the choice of the center and width of the RBFNN greatly affects the performance of the adaptive neural network controller, appropriate radial basis function must be selected to guarantee the approximation accuracy. Here we choose the Gaussian function as the radial basis function whose expression is

$$\xi_i(x) = e^{-\frac{\|x-\mu_i\|^2}{2\sigma_i^2}}, i = 1, 2, \cdots n \tag{44}$$

where σ_i is the width of the Gaussian function, μ_i is the center vector of the Gaussian function, and n is the number of nodes in the hidden layer. The RBF neural networks are selected in the simulation as follows. The structure of the first RBFNN is 1-9-1, the network input is x_1, and the network weights are initialized to 0, $\mu_1 = [-5\ -3\ -2\ -1\ 0\ 1\ 2\ 3\ 5]$. The structure of the second RBFNN is 2-9-1, the network input is x_1 and x_2, $\mu_2 = \begin{bmatrix} -9 & -7 & -5 & -3 & 0 & 3 & 5 & 7 & 9 \\ -9 & -7 & -5 & -3 & 0 & 3 & 5 & 7 & 9 \end{bmatrix}$, and the network weights also are initialized to 0. The initial flight path angle is $-3°$.

The simulation results are presented in Figs. 2 to 4, where Fig. 2 shows the tracking results for the state variables γ, Fig. 4 shows the control input δ_e. From the Fig. 3 we can see that the tracking performance is very good, only with very limited tracking error in the initial period of time.

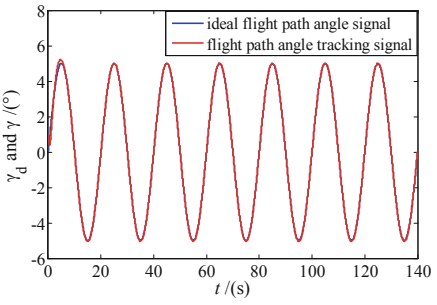

Fig. 2. The flight path angle tracking result in case 1

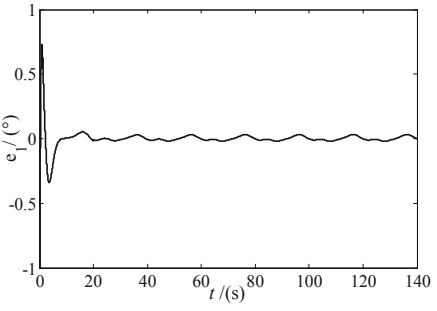

Fig. 3. The tracking error of the flight path angle in case 1

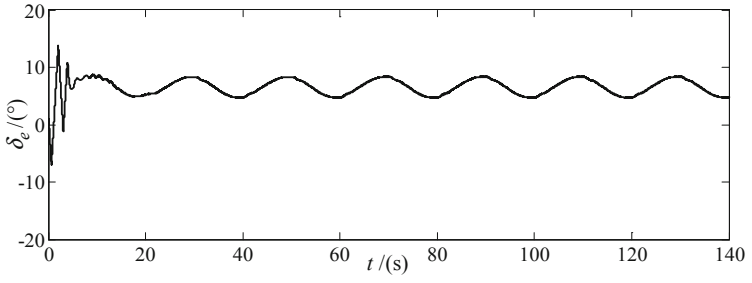

Fig. 4. The elevator deflection angle in case 1

5.2 Case 2: The Non-nominal Situation

In this simulation case, the parameters uncertainty and time-varying external disturbances are considered. The aerodynamic parameters $C_{m0}, C_{mq}, C_{m\alpha}, C_{m\dot{\alpha}}, C_{m\delta_e}, C_{L0}, C_{L\alpha}$ are set to be between −20% and 20% deviation from nominal values, respectively. And the time-varying external disturbances are set as: $d(t) = 0.1\sin(t)\cos(t)$. The control parameters are unchanged.

The simulation results are presented in Figs. 5, 6, 7, 8 and 9. Although the tracking error of flight path angle is bigger than case1, it is limited in an acceptable range by the controller and the convergence speed is fast. Comparing with the case 1, the states tracking results in this case all have some little oscillation due to the time-varying icing influence and external disturbances. The elevator deflection angle generated by controller is shown in Fig. 9. It can be seen that comparing with case 1, the elevator deflection angle also has some oscillation because of the disturbances.

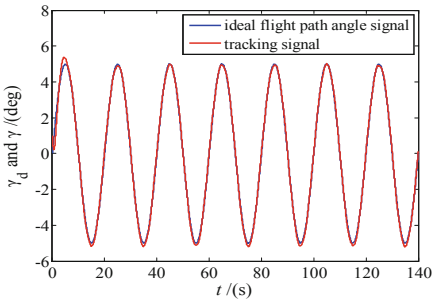

Fig. 5. The flight path angle tracking result in case 2

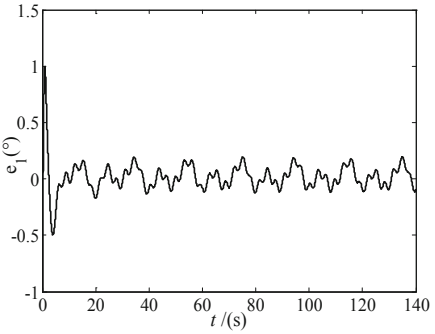

Fig. 6. The tracking error of the flight path angle in case 2

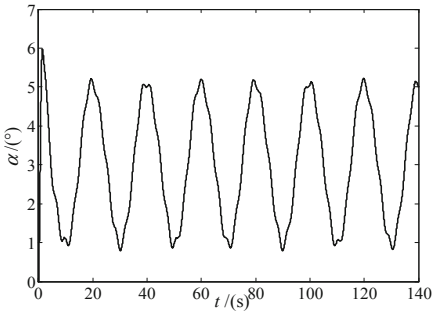

Fig. 7. The angle of attack in case 2

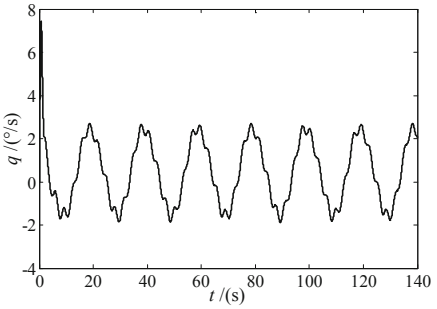

Fig. 8. The pitch rate in case 2

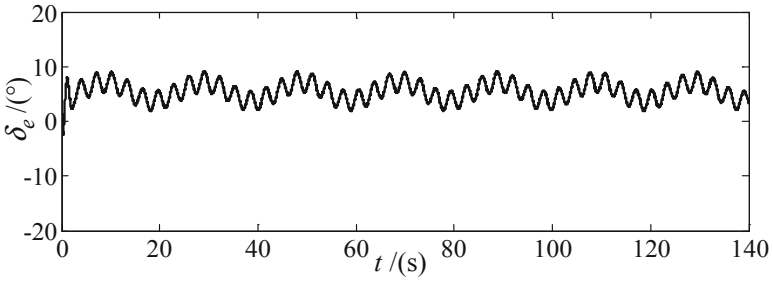

Fig. 9. The elevator deflection angle in case 2

From simulation results of the two cases, we can see that the control method proposed in this paper make a faster convergence speed, and the steady-state error is small even if there is time-varying external interference and modeling error, and effectively eliminates the chattering phenomenon of the control input.

6 Conclusion

A adaptive backstepping terminal sliding mode control method for the control of flight-path angle has been developed. The last step of the design of controller adopts a special non-singular terminal sliding mode to replace the traditional linear sliding mode. The control strategy based on non-singular terminal high-order sliding mode control law is designed to remove the chattering, and make the last state of the system converge in a finite time. It is proved by Lyapunov method that all signals in the closed-loop system are semi-global uniform ultimately bounded. At last, the numerical results of two simulation cases validate the viability of this approach.

References

1. Luo Y, Yoo HY, Ishihara A (2013) Adaptive backstepping design for a longitudinal UAV model utilizing a fully tuned growing radial basis function network. In: AIAA 2011, p 1451
2. Wang YN, Chen K, Wen-Xing FU (2016) Hypersonic flight vehicle's flight path angle tracking control with attack angle constraints. J Solid Rocket Technol 1:125–130
3. Wang S, Xu B, Sun F (2012) Discrete neural altitude control for hypersonic vehicle via flight path angle tracking. Res J Appl Sci Eng Technol 4(20):3930–3936
4. Guo Y, Liu J (2013) Neural network based adaptive dynamic surface control for flight path angle. In: Decision and control. IEEE, pp 5374–5379
5. Sharma M (2002) Flight-path angle control via neuro-adaptive backstepping. In: American control conference. In: AIAA 2002, p 4451
6. Sun XX, Liu X, Xu S (2015) Nonlinear gains recursive sliding mode control for flight-path angle of UAVs. Syst Eng Electron 37(2):379–384
7. Kanellakopoulos I, Kokotovic PV (1991) Systematic design of adaptive controller for feedback linearizable systems. IEEE Trans Autom Control 36(11):1241–1253

8. Kristic M, Kanellakopoulos I, Kokotovic PV (1992) Adaptive nonlinear control without overparametrization. Syst Control Lett 19(2):177–185
9. Kristic M, Kanellakopoulos I, Kokotovic PV (1995) Nonlinear and adaptive control design. Wiley, New York
10. Dong W, Sun X, Lin Y (2006) Adaptive backstepping control: development and applications. Control Decis 21(10):1081–1086
11. Wu Z-J, Xie X-J, Zhang S-Y (2005) The reduced-order design of robust adaptive backstepping controller. Acta Autom Sin 31(4):543–548
12. Guan C, Zhu S (2005) Multiple sliding mode robust adaptive control of an electro-hydraulic servo system. Control Theory Appl 22(6):931–938
13. Gu W, Zhao H, Pan C (2005) Sliding mode control for an aerodynamic missile based on backstepping design. J Control Theory Appl 3(1):71–75
14. Li J, Xu D (1999) Adaptive sliding mode controller for nonlinear systems with mismatched uncertainties based on adaptive backstepping scheme. Control Decis 14(1):46–50
15. Yan M, Xu H, He Y (2004) Adaptive sliding mode control based on tuning function for nonlinear systems with triangular structure. Control Theory Appl 21(5):840–843
16. Bartolini G, Ferrara A, Giacomini L et al (2000) Properties of a combined adaptive/second-order sliding mode control algorithm for some classes of uncertain nonlinear systems. IEEE Trans Autom Control 45(7):1334–1341
17. Hanke CR, Nordwall DR (1970) The simulation of a jumbo jet transport aircraft. Volume 2: modeling data/detail: NASA-CR-114494. NASA, Washington, D.C